Ar L-shell Auger-electron emission in ion-solid collisions

Fang Xu and Assunta Bonanno
Dipartimento di Fisica, Universitá della Calabria, 87036 Arcavacata di Rende, Cosenza, Italy
(Received 22 October 1991; revised manuscript received 1 June 1992)

Ar L-shell Auger-electron emission has been studied by bombarding Si, Ti, and condensed Ar surfaces with 5–15-keV Ar^+ ions. Our spectra show clear evidence for ion-solid interactions. The eventual $3p$ vacancies of most of the outgoing inner excited Ar particles are filled by the solid valence electrons but some of them can still survive such a charge-transfer process. The Auger electrons emitted in the vacuum will give rise to well-separated $L_{23}MM$ and $L_{23}M_{23}$-M^3 peaks in the observed spectra. The neutralization probability strongly depends on the nature and condition of the target surface and a large variation of the relative intensities has been observed by changing the effective thickness of the Ar layer condensed on an Al substrate. Spectra obtained for Ar^+-Si, Ar^+-Ar, and Ar^+-Ti systems show very different and strongly primary energy-dependent intensity ratio between various L_{23} peaks suggesting a great influence of the solid environment on the relative transition rates. Further, our results show that the $L_{23}M_1M_{23}$ to $L_{23}M_{23}M_{23}$ intensity ratio for an inner excited Ar atom moving in a solid can be substantially different from that for a stationary atom embedded in the bulk matrix. Some weak Auger features in the high-energy spectral regions have also been observed and identified. A vacancy-transfer mechanism involving a two-electron process has been proposed for the Ar $2p$ electron promotion in Ar-Si collisions.

I. INTRODUCTION

Auger-electron spectra taken with ion bombardment on solid surfaces show both similarities and differences with those obtained in gas-phase ion-atom collisions.[1–4] Though in both cases the basic physical mechanism for core electron excitation is generally interpreted within the framework of the electron promotion model of Fano and Lichten[5] and Barat and Lichten,[6] the deexcitation processes can be quite different from each other. It has been shown that in the case of ion-solid interactions a great number of decays take place in the solid matrix involving two valence electrons and the relative transition probabilities of various decay channels can be substantially different from those in the gas-phase experiments. Further, there exists a variety of interesting phenomena, such as surface neutralization and ionization,[7,8] which are unique to the ion-solid interactions and can alter considerably the detected electron spectra.[9,10]

Though Ar L-shell Auger-electron emission has been extensively studied in ion-atom experiments for more than two decades because of its prototypical role in understanding of the collisional inner excitation mechanism,[11–15] its counterpart in ion-surface measurements has received relatively little attention and identifications of many spectral features are not clear yet. Observation of projectile Ar Auger electrons has been reported for Ar^+-transition metal and Ar^+-Si systems.[16–20] It was found that the Ar Auger yield is anomalously higher for this latest than for Ar^+-Mg and Ar^+-Al through the concentration of implanted Ar is nearly the same.[17] The mechanism of Ar inner-shell electron excitation in these Ar^+-lighter element systems still remains a controversial issue.[16,17,20]

In this paper we report a detailed study on the Ar L-shell Auger-electron emission during Ar^+ ion bombardment on Si and Ti surfaces and on condensed Ar layers. Our results show clear ion-solid interaction effects in the observed Ar Auger line shape. In particular, we show that the eventual $3p$ holes of most of the inner-shell excited leaving Ar particles are neutralized by capturing solid valence electrons, but some of them can still survive such a surface neutralization process. The subsequent Auger decays in the vacuum result in the normal $L_{23}MM$ lines and the satellite $L_{23}M$-M^3 peaks in the detected spectra (throughout this paper we will adopt the notation *AB-CDE* to indicate an Auger transition with initial vacancies in A and B shells and a final state with holes in C, D, and E levels). The charge-transfer probability depends on the nature and conditions of the target surface and a large variation of the Ar line shape has been observed by changing the effective thickness of the Ar layers condensed on an Al metal substrate. We show that the surrounding solid environment has a large influence on the relative transition cross sections not only for a stationary atom embedded in the solid matrix but also for a moving atom traveling inside the solid. We propose an interpretation invoking a two-electron process for the Ar $2p$ excitation in the Ar-Si system.

This paper is organized as follows: In the next section we will briefly describe our experimental setup and the measurement conditions. In Sec. III we present our results together with a detailed discussion for the systems Ar^+-Ar, Ar^+-Si, and Ar^+-Ti. Finally, some salient remarks and conclusions of this study are summarized.

II. EXPERIMENT

The experiments were conducted in a UHV chamber with a base pressure in the mid 10^{-10} Torr and it rose to

the 10^{-9} Torr range during beam operation. A differentially pumped A-DIDA Atomika ion gun was used to produce an Ar^+ ion beam with a spot size of 0.6–1 mm and an ion current varying from 10 to 80 $\mu A/cm^2$. For the gas discharge voltage used (70 V), a small portion of Ar^{2+} ions (<5% according to the manufacturer's specification) was contained in the primary beam which was not mass analyzed. An electron gun was also employed for comparative studies. All the incidence and emission angles are referred to the surface normal. The emitted electrons were collected with a hemispherical energy analyzer (acceptance angle ~25°) situated at 70° from the incidence direction ($\theta_i+\theta_e=70°$) and working in a constant pass energy mode (PE=100 eV) and for spectra recorded in the derivative mode a peak-to-peak modulation voltage of $V_{pp}=2$ V was used. All the measured kinetic energies are referred to the Fermi level. Though the overall resolution was about 2.5 eV the accuracy in determining the energy difference was between 0.2 and 2 eV depending on the statistical quality of the spectra.

The Si and Ti samples were mounted on a manipulator which could be rotated to change the incidence angle. Samples were cleaned by *in situ* ion sputtering. Small traces of carbon were found in Mg and Ti even after a prolonged sputtering. Ar layers were obtained by condensing pure Ar gas, introduced through a gas line inside the chamber and about 8 mm away from the sample, onto a polycrystalline Al disk attached on a cold finger of a cryostat with He cycling. An Fe-Au thermocouple was used to monitor the sample temperature. The Al substrate also served for beam alignment. Only thin layers of Ar were used in this study and the Al *LMM* signals were constantly monitored to ensure that no surface charging occurred during the experiment. Because of the destructive nature of the ion sputtering process itself and the strong dependence of the frozen layer thickness on the substrate temperature which could be altered by the impact of energetic projectiles, it was necessary to operate in a dynamically equilibrium situation (with beam and ion pumps on and gas line open) and the variation of the condensed Ar layer thickness was achieved by changing either the local Ar pressure or the incidence ion beam current.

III. RESULTS AND DISCUSSIONS

A. The case of Ar^+-Ar

In Fig. 1 are shown some typical Ar Auger-electron spectra taken in the $N(E)$ mode for electron and Ar^+ ion bombardment on thin frozen Ar layers along an incidence angle of 45° relative to the surface normal. These spectra have been secondary-electron background subtracted, analyzer transmission factor corrected, and peak height normalized. The main *L*-shell Auger feature is peaked at around 208 eV and a broad structure extends to below 150 eV. The broad structure extending to low energies is definitely not caused by surface charging but may contain a large number of Doppler broadened unresolved transition lines and possible energy losses for electrons traveling inside the solid.

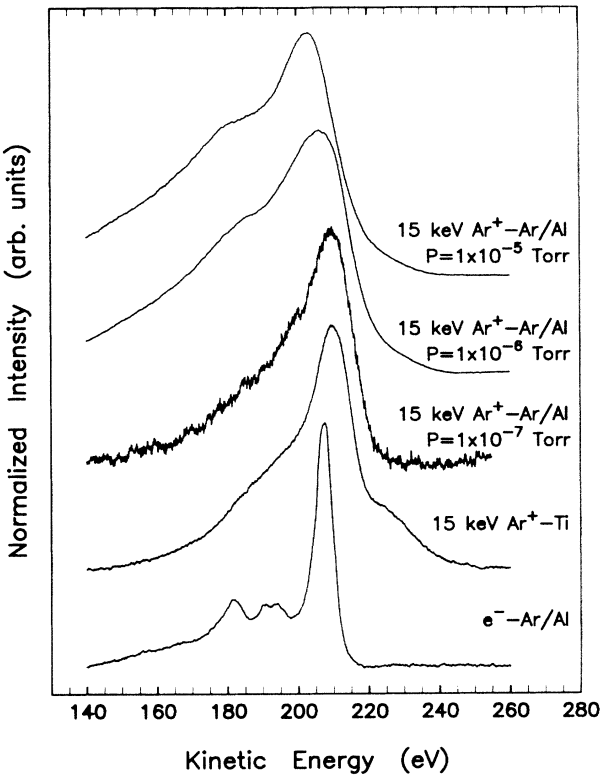

FIG. 1. Ar *L*-shell Auger spectra for 15-keV Ar^+ ion bombardment on Ti, Ar layers with different thicknesses (expressed in argon residual pressure in the chamber), and for 1.8-keV electron impact on frozen Ar ($T=21$ K). The incidence angle is 45° relative to the surface normal. All the spectra have been analyzer transmission factor corrected, secondary-electron background subtracted, and peak height normalized.

We note that these spectra differ very much from what was observed in gas-phase Ar^+-Ar experiments.[21,22] Presumably for the signal intensity reason, to our knowledge, no Ar Auger spectrum is available in the literature for the Ar^+-Ar system taken at low collision energies (<20 keV) for comparison with our ion-solid experiments. However, if the collision energy is sufficiently high then simultaneous inner- and outer-shell electron excitation will occur so that the LM^iLM^{i+2} transitions at kinetic energies lower than ~196 eV will dominate in the Ar Auger spectra.[21,22] Though such multielectron excitation is still possible in our case their contributions should be quite small relative to the singly excited *LMM* peak.

In Fig. 2 we present a series of normalized derivative spectra excited by impinging Ar^+ ions and 1.8-keV electrons on Ar layers condensed on an Al substrate held at a temperature of $T=22$ K. We note that for a fixed experimental geometry, the thickness of the condensed Ar layer depends on the combination of the local Ar partial pressure which is one or two orders higher than, but proportional to, the measured chamber pressure *P*, the sticking coefficient which increases with decreasing substrate temperature, and the sputtering efficiency which is related to the beam current density and the primary ion energy. A quantitative estimate of the amount of condensed

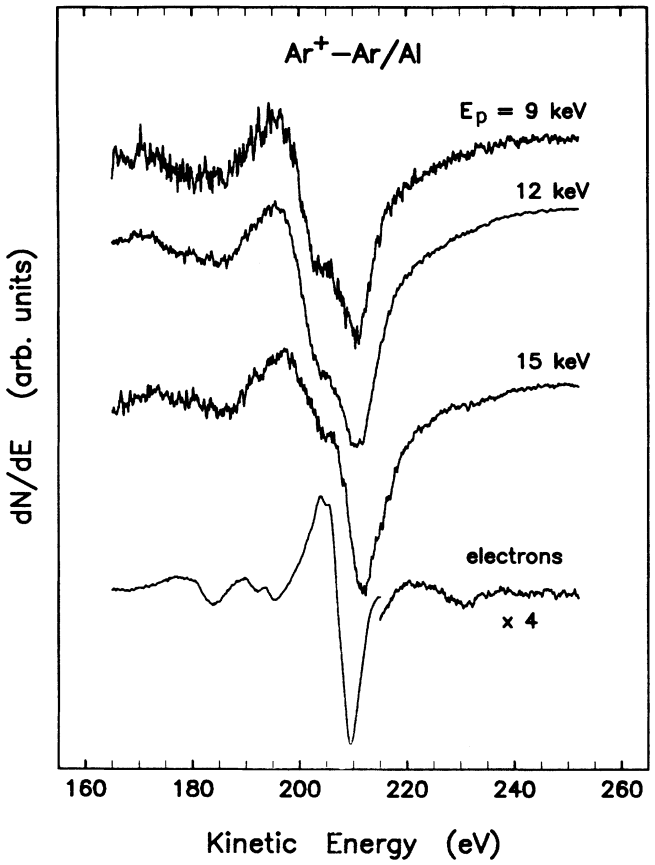

FIG. 2. Normalized Ar L-shell Auger spectra for Ar^+-Ar taken in the derivative mode at $\theta_i = 45°$ for several incident ion energies with a beam current of $I = 10\ \mu A/cm^2$, a chamber pressure of $P = 6 \times 10^{-6}$ Torr, and a substrate temperature of $T = 22$ K. The bottom-most curve is that obtained by 1.8-keV electron impact.

Ar was not possible through the measurement of either substrate or overlayer spectroscopic signals since the covering up of the deposited layer not only influences the detection of Auger electrons but also affects directly the core excitation process itself. However, the observation of the surface neutralization effects (see below) would lead us to qualitatively estimate the amount of deposited Ar to be from a fraction of a monolayer to a few monolayers (in dynamically equilibrium situations).

Let us first discuss the Ar Auger features in the spectrum obtained by electron stimulation. In this paper all the experimental peak energies in the derivative spectra are referred to the positions of the negative cursors unless otherwise specified and the observed Auger peaks are listed in Table I for comparison with different collision systems. The most prominent peak at 209.4±0.2 eV (errors are relative to the statistical uncertainty) is ascribed to an $L_{23}M_{23}M_{23}$ transition. The linewidth of 5.6 eV, determined from the separation between the positive and negative cursors, is essentially due to the superposition of six unresolved Auger lines with different spin-orbit configurations[23] and a possible, but relatively small broadening due to the solid-state effects.

The doublet at 192.1±0.2 and 195.0±0.2 eV is attributed to $L_3M_1M_{23}$ and $L_2M_1M_{23}$ decays, respectively. The width of ~2.2 eV can be accounted for by the limited energy resolution of our spectrometer. The peak seen at 183.7±0.3 eV is an L_2 transition involving two $3s$ electrons. The other similar peak with an initial L_3 hole at lower kinetic energy is not well resolved but two positive cursors at 180.6±0.3 and 176.7±0.3 eV can be clearly seen in our spectrum. This may be caused by a possible overlap with many shake-off lines having similar intensities in this energy region.[23]

The relatively broad feature at 231±2 eV can be ascribed to an $L_{23}M_{23}V$ transition involving a valence elec-

TABLE I. Observed Ar L-shell Auger and autoionization electron peak energies (referred to the position of the negative cursor in the derivative spectra). (The projectile Ar^+ ion energy is $E_p = 15$ keV and the incidence angle is $\theta_i = 45°$ with respect to the surface normal whereas for electron impact $E_p = 1.8$–2.7 keV and $\theta_i = 30°$.)

Transition							
Initial state	Final state	e^--Ar/Al	Ar^+-Ar/Al	e^--Ar (Si)	Ar^+-Si	e^--Ar (Ti)	Ar^+-Ti
$2p^{-1}3p^{-1}$	$3s^{-2}3p^{-1}$	168±2					169±2
$2p^{-1}$	$3s^{-2}$	179.8±0.3[a] 183.7±0.3	187.9±0.6		182±2	181±2	185±2
$2p^{-1}$	$3s^{-1}3p^{-1}$	192.1±0.2 195.0±0.2	199.0±0.6	195.3±0.8	193.7±0.8	197±2	194±2
$2p^{-1}$	$3p^{-2}$	209.4±0.2	213.5±0.4	212.0±0.5	210.6±0.5	211.9±0.5	214.9±0.5
$2p^{-1}3p^{-1}$	$3p^{-3}$		207±1				
$2p^{-1}4s^{+1}$	$3p^{-2}4s^{+1}$				222±1		
$2p^{-1}3d^{+1}$	$3p^{-2}3d^{+1}$				225±1		
$2p^{-1}4s^{+1}$	$3p^{-1}$					227±2	228±1
$2p^{-1}$	$3p^{-1}V^{-1}$	231±2	233±2			227±2	228±1
$2p^{-2}4s^{+1}$	$2p^{-1}3s^{-1}$						233±1
$2p^{-1}$	V^{-2}			239±2		239±1	

[a]This position is estimated from the separation between the positive cursors of $L_2M_1M_1$ and $L_3M_1M_1$ peaks.

tron of the underlying metal or to an $L_{23}M_{23}N_1$ autoionization transition leading to a final +1 charge state. The estimated upper limit of the kinetic energy for the $L_{23}M_{23}V$ ($L_{23}M_{23}N_1$) Auger electrons should be about 22–24 (22) eV with respect to the $L_{23}M_{23}M_{23}$ one, in very good agreement with the observed peak position. However, the linewidth of ~10 eV (see the amplified portion of the spectrum in Fig. 2) would favor the assignment to $L_{23}M_{23}V$. We point out that interatomic transitions, already observed previously for TiO_2 (Ref. 27), should be much less probable than intra-atomic ones but at present time seem to be the only possible assignment.

The small and rather broader structure at ~168 eV is quite difficult to be identified. In both electron-Ar (Ref. 23) and H^+-Ar (Refs. 11–13) gas-phase experiments many weak transition lines have been observed but not identified. It is commonly assumed that these lines are due to transitions from an initial $2p^{-1}3s^{-1}$ state to a final $3s^{-2}3p^{-1}$ configuration.[13,28]

The Auger spectra obtained by ion bombardment are much more complicated and less resolved. The main $L_{23}M_{23}M_{23}$ peak is shifted to 213.5±0.4 eV for $E_p=15$ keV and to 210.9 eV for $E_p=9$ keV (Fig. 3). We point out that the kinetic energy of the Auger electrons emitted in free space can somehow differ from that emitted in the solid and can also acquire a substantial and primary energy-dependent upward Doppler shift, an effect that must be taken into account in comparisons with theoretical predictions.

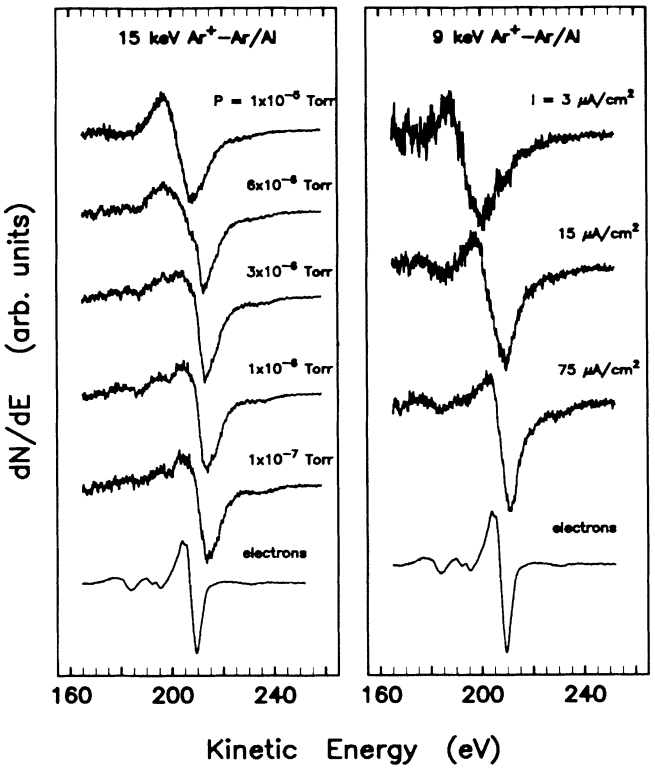

FIG. 3. Normalized Ar L-shell Auger spectra obtained by bombarding frozen Ar layers with 15-keV Ar^+ ions for different amounts of deposited Ar (left panel) and 9-keV Ar^+ ions for three different beam currents (right panel). The Ar layer thickness is measured with the chamber partial pressure. The substrate temperature is 21 K and the beam current is $I=10$ $\mu A/cm^2$ for the curves in the left panel and the substrate temperature is 23 K and the chamber pressure is 3×10^{-6} Torr for those in the right panel. The bottom-most spectra are those for electron stimulation.

The most interesting observation is the appearance of a large shoulder at the low-energy side of the main peak, absent in the electron-induced spectrum. It shows a strong dependence on Ar coverage. To understand the nature of this component we varied the amount of deposited Ar by changing either the Ar partial pressure or the ion beam current while keeping all other experimental parameters constant. Two sets of results of such measurements are presented in Fig. 3. For thin Ar overlayers, the spectral shape is quite similar to, though somehow shifted with respect to, that for electron impact, but for thick layers the intensity of the main $L_{23}M_{23}M_{23}$ peak is greatly reduced while the above-mentioned structure appears at 207±1 for $E_p=15$ keV (200±1 eV for $E_p=9$ keV) as a well distinct peak. Even for the highest coverage investigated, the position of this latter is still severely affected by a partial overlap with the $L_{23}M_{23}M_{23}$ feature. For intermediate thicknesses, the overall line shape is a result of the superposition of these two components.

The regular variation of the relative intensity of this feature with respect to the $L_{23}M_{23}M_{23}$ peak as a function of the Ar layer thickness lead us to argue that it should be related to the interactions between projectile ions and the substrate. In particular, we propose the following description for a small quantity of Ar deposition: the eventual $3p$ vacancies of most of the outgoing inner-shell excited Ar particles (originally present in the projectiles and not neutralized before collision, or created in a target atom due to a resonant charge transfer to the projectile ion, or simultaneously ionized in either projectile or target species during encounter) are neutralized by the substrate conduction electrons via an Auger neutralization or a resonant tunneling process so that they have all outer shells filled.[7,8] Given that the work function of clean Al is much smaller than the Ar first ionization potential, such a neutralization mechanism is energetically allowed and greatly favored and the decay of these particles results in the $L_{23}M_{23}M_{23}$ transition seen at 213.5 eV for $E_p=15$ keV (210.9 eV for $E_p=9$ keV). For high Ar coverages, the electron capture from the underlying Al substrate for the incoming and outgoing Ar ions becomes inhibited because of the covering up (the portion of the projectile Ar^+ ions being neutralized by the substrate conduction electrons depends, of course, on the effective frozen Ar layer thickness). The equal probability of the $2p$ electron promotion further suggests that in Ar^+-Ar collisions at least half of the inner-shell excited projectile or target Ar particles should have a hole in their outer shells. These scattered inner-shell-excited Ar particles will undergo an $L_{23}M_{23}$-M_{23}^3 Auger transition resulting in a +3 final charge state.[29]

To get a further insight into the deexcitation processes we performed a simple kinematical calculation on the

cross section ratio between the ejected core excited projectile and target particles in the primary collisions using the classical mechanics for the case of $E_p=9$ keV and $\theta_i=45°$ using the Molière approximation to the Thomas-Fermi potential with a Firsov screening length. The results indicate that actually no excited atoms should leave the surface to decay in the vacuum if the critical minimal approach distance for $2p$ electron excitation is taken to be less than 0.303 Å, a value much larger than the threshold distance found in gas-phase experiments (0.25–0.26 Å, Ref. 30). Therefore, we conclude that in this particular case the target atoms excited in the primary collisions cannot be directly ejected.

The other Auger features at lower energies behave in a quite similar way as the deposited Ar layer thickness varies. All the distinct lines observed in the electron-induced spectrum are smeared out and only broad structures can be seen. A further cause of this behavior is the Doppler broadening due to the fast movement of the parent excited Ar relative to the analyzer, an effect absent in the case of electron impact.

The high-energy peak at $\sim 233\pm 2$ eV cannot be discerned for large Ar deposition. This peak may be due to $L_{23}M_{23}V$ or $L_{23}M_{23}N_1$, as in the case of electron impact. However, for an Ar atom with a $2p$ vacancy the $4s$ binding energy (4.2 eV, Ref. 25) is very close to the work function of the clean Al (4.28 eV, Ref. 24) and should be somehow reduced by a few tenths of eV in the vicinity of a solid surface.[31] Therefore, we can exclude the origin of the $L_{23}M_{23}N_1$ transition. The disappearance of this feature at high Ar coverages is consistent with the $L_{23}M_{23}V$ assignment.

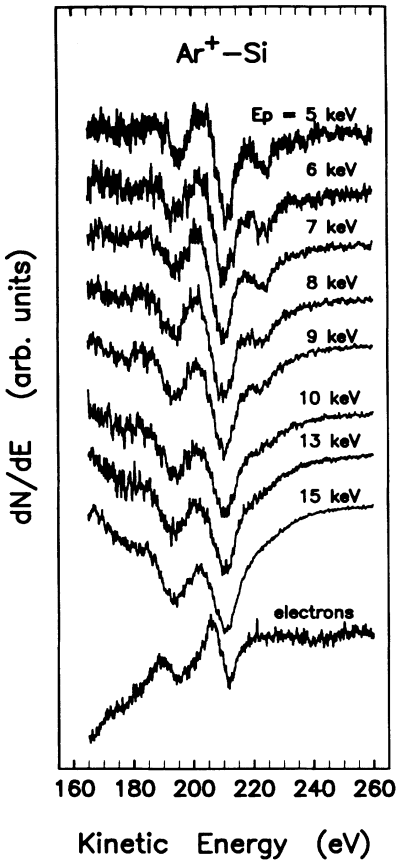

FIG. 4. Normalized Ar L-shell Auger spectra for Ar^+ impact onto a Si substrate for several primary ion energies. The incident angle is 45° relative to the surface normal.

B. The case of Ar^+-Si

In Fig. 4 we show a set of Ar L-shell Auger spectra for Ar^+ on a single-crystal Si(111) surface at an incidence angle of $\theta_i=45°$. The orientation of the sample has no particular meaning in our experiments because of the rapid amorphization of the surface. To better emphasize the line-shape changes, all the spectra have been normalized. The bottom-most curve is that obtained by electron impact on Ar implanted in Si.

We first note that the electron-induced Auger spectrum (EIAS) of Ar embedded in the Si matrix is somehow different from that obtained for condensed Ar (see the upper panel of Fig. 5). The most intense $L_{23}M_{23}M_{23}$ peak is shifted by about 2.6 eV toward high energies though its linewidth remains unaltered. This suggests that the interactions with the surrounding Si environment result in a change of its energy levels. The spin-orbit components of the $L_{23}M_1M_{23}$ and $L_{23}M_1M_1$ peaks are no longer resolved and we notice a large increase of the relative intensity of the $L_{23}M_1M_{23}$ peak with respect to the most prominent $L_{23}M_{23}M_{23}$ in comparison with the case of frozen Ar, indicative of a strong influence of the matrix also on the relative transition rates. The broad feature seen at 239 ± 2 eV can be attributed to an interatomic $L_{23}VV$ transition in which the Ar $2p$ vacancy is filled by a Si valence electron and another valence electron is ejected.

For the Auger spectra produced by ion bombardment the energy positions of the negative and positive cursors of the most intense peak $L_{23}M_{23}M_{23}$ are shifted for about 1–1.4 eV and 4 eV, respectively, toward lower energy. We suggest that this peak is actually an overlap of three contributions. The first one is the $L_{23}M_{23}M_{23}$ decay occurring in the Si matrix having a similar kinetic energy as that in the EIAS. The second one is due to the same transition but decaying outside the sample, thus with a possible, though probably quite small, Doppler shift. The third component contributing to the low-energy part of the peak is the $L_{23}M_{23}$-$M_{23}{}^3$ transition resulting from the deexcitation of the Ar^{2+} ions with $3p$ holes not neutralized by the surface electrons.

The most evident difference in the spectral shape between the Ar^+-Si and Ar^+-Ar cases probably is the large intensity of the $L_{23}M_1M_{23}$ peak relative to the $L_{23}M_{23}M_{23}$ one and its variation as a function of the primary ion energy (see Fig. 4 and the lower panel of Fig. 5). The dramatic increase of this intensity ratio (estimated from the product of the peak height and width) versus the primary energy, plotted in Fig. 6, is very different from the behavior observed for other light elements. If we consider that the relative probabilities of various decay channels are independent on the excitation events and on the surface nature and conditions if occurring in

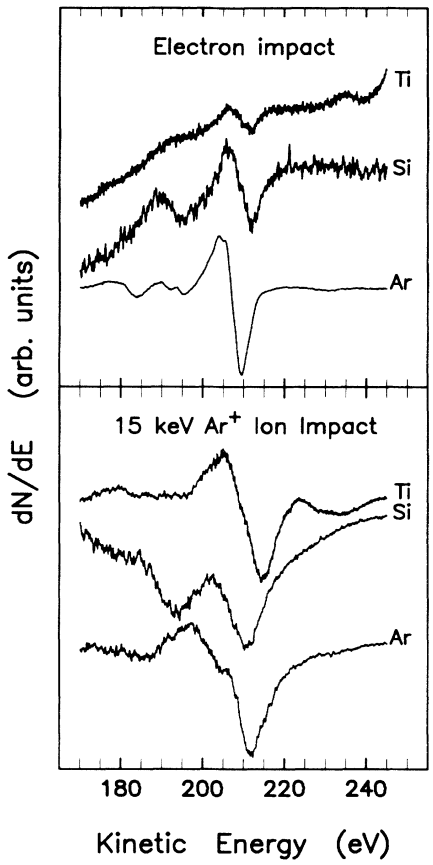

FIG. 5. Comparison of Ar Auger-electron spectra for three different systems under electron (upper panel) and 15-keV Ar^+ ion (lower panel) impact.

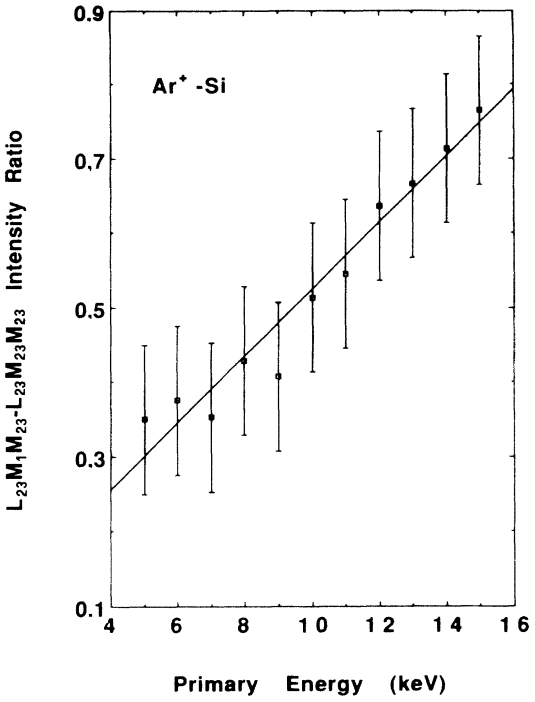

FIG. 6. The intensity ratio between the $L_{23}M_1M_{23}$ and $L_{23}M_{23}M_{23}$ peaks, estimated from the product of the peak height and width, vs the primary Ar^+ ion energy. The line is a linear fitting and only serves to guide eyes.

vacuum, then we would expect the intensity ratio between $L_{23}M_1M_{23}$ and $L_{23}M_{23}M_{23}$ peaks for any ion-induced spectrum for Ar^+-Si to be intermediate between the limits determined by electron stimulation for solid and gas Ar targets. For this latter case, Werme *et al.* showed a ratio of 1:4 (Ref. 23). The results shown in Fig. 4 evidently contradict such expectations. The large intensity ratio suggests that a great part of the decay processes must have occurred inside the solid and the relative transition rates are drastically altered for an inner-shell-excited Ar particle moving in the Si bulk matrix relative to those for a rest atom. The observed dramatic increase of this ratio versus the primary energy (Fig. 6) further indicates an increase of the deexcitation events inside the solid relative to those in the vacuum and a substantial influence of the solid environment on the deexcitation channels favoring decays involving one $3s$ electron rather than two $3p$ electrons. These results clearly demonstrate the peculiarities of the ion-solid collisional excitation and deexcitation processes with respect to the gas-phase ion-atom collision experiments, especially in regard to the relative transition rates.

Another salient feature of the spectra shown in Fig. 4 is the behavior of the high-energy peaks at 222 ± 1 and 225 ± 1 eV. The presence of two narrow peaks instead of one broad peak in the spectra can be clearly inferred by observing the changes in line shape and peak energy as a function of E_p (we note that no such changes are detected for the main $L_{23}M_{23}M_{23}$ and $L_{23}M_1M_{23}$ peaks). Their intensities relative to the main $L_{23}M_{23}M_{23}$ peak decrease monotonously as the primary energy increases from 5 to 10 keV and they can no longer be distinguished from the background for $E_p \geq 12$ keV. These features were not resolved in previous studies[17,20] but the overall behavior is in good agreement. In gas-phase experiments such high-energy peaks were usually assigned to autoionization decays in a neutral Ar atom with one $2p$ hole and one electron added to the outer shell[11] ($L_{23}M_{23}N_1$) or to autoionization from an initially highly M-shell ionized Ar atom[15] (initial state $2p^{-1}3p^{-5}3d$ or $2p^{-1}3p^{-5}4s$), whereas in ion-solid experiments they were assigned to the L_{23}^2 Auger transitions with a double initial vacancy in the L-shell L_{23}^2-$L_{23}M_1M_{23}$ (Ref. 16) and L_{23}^2-$L_{23}M_{23}^2$ (Ref. 18).

We point out that direct ionization of many Ar outer-shell electrons is unlikely at our low collision energies and that a multiple charge transfer from Ar atoms to the solid is energetically forbidden. According to the calculations of Larkins,[32] the kinetic energy for the L_{23}^2-$L_{23}M_{23}^2$ peak should be 12 eV relative to the $L_{23}M_{23}M_{23}$ peak. However, as we shall discuss in detail later on, for low-energy collisions as in our case, the molecular-orbital model[6] predicts that in an Ar-Si asymmetric collision only $2p$ core electrons of the lighter partner (Si) could be excited while in an Ar-Ar symmetric collision core vacancies would most probably be shared equally between the alike partners. The same argument

can be applied to the L_{23}^2-$L_{23}M_1M_{23}$ transition, whose energy should be around 199 eV.

Calculations based on the experimental binding energies[25,26] predict that transitions from initial $2p^{-1}4s^{+1}$ and $2p^{-1}3d^{+1}$ states to final $3p^{-2}4s^{+1}$ and $3p^{-2}3d^{+1}$ states (with the electron in the high-lying autoionizing state as a spectator) should have kinetic energies of 218 and 222 eV, respectively, relative to the vacuum level. The fact that the binding energies of the $4s$ and $3d$ levels for an inner-shell singly ionized Ar (4.2 and 1.7 eV, respectively[25]) are smaller than the Si work function (4.6 eV) excludes an atomic decay since the electron eventually present in these outer shells most probably will be resonantly transferred to the solid during the escape from the surface. However, if the deexcitation takes place inside the solid then such transitions have quite correct positions. Indeed, their relative energies of 11.4 and 14.4 eV with respect to the main $L_{23}M_{23}M_{23}$ one are in good agreement with the theoretical predictions of 12 and 16 eV, respectively.

Now we discuss the mechanism for Ar $2p$ core electron excitation in the Ar-Si system. Fig. 7 shows the Ar $L_{23}M_1M_{23}$ ($L_{23}M_{23}$-$M_1M_{23}^2$), $L_{23}M_{23}M_{23}$ ($L_{23}M_{23}$-M_{23}^2), and the total Auger intensities as a function of the primary ion energy, intensities estimated from the product of the peak-to-peak height and the linewidth

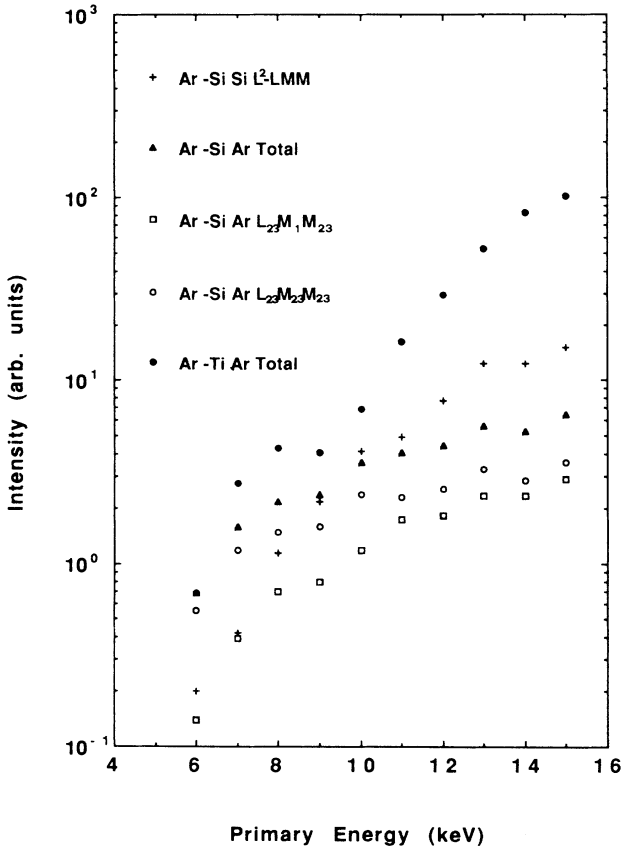

FIG. 7. Ar L-shell Auger intensities obtained for the Ar^+-Si and Ar^+-Ti cases as a function of the projectile energy. For comaprison, the intensity of the Si L^2-LMM peak is also plotted.

for the shape of each individual component does not vary sensitively. The Si L_{23}^2-$L_{23}M_{23}^2$ intensity is also plotted for comparison. These results are in qualitative agreement with those reported by Viaris de Lesegno and Hennequin[17] but differ very much from those of Wittmaack.[20] Such difference may be partially caused by the possible, though small, Ar^{2+} contamination in our Ar^+ beam, as discussed in detail by Baragiola, Nair, and Madey.[33]

Kempf and Kaus[16] suggested that the Ar $2p$ vacancy is created exclusively by the collisions between the impinging Ar ions and the preimplanted Ar atoms. Wittmaack,[20] instead, argued that the asymmetric collisions between Ar and Si atoms are responsible for the excitation of the L-shell electron in Ar. Viaris de Lesegno and Hennequin[17] proposed an Ar M-shell to Si L-shell vacancy transfer mechanism through $3s\sigma$-$3p\pi$-$3d\sigma$ molecular-orbital rotational couplings.

According to the molecular-orbital (MO) curve crossing model, in an Ar-Si collision the L-shell electron in Ar can be promoted only through $3d\sigma$ rotational couplings. The threshold for such excitation mechanism in Ar^+-Ar collisions has been determined as $R_{\min}=0.13$ Å (Ref. 34), which corresponds to 28 keV of the projectile Ar^+ ion energy for head-on collisions. In the case of Ar-Si, no experimental data exist but the threshold value should be very close to that for Ar^+-Ar. If we take $R_{\min}=0.14$ Å then $E_{\text{thresh}}=24$ keV and if we take $R_{\min}=0.16$ Å then $E_{\text{thresh}}=19$ keV [the MO correlation diagram predicts a $R_{\min}\sim 0.1$ Å (Ref. 35)]. Therefore, the model proposed by Viaris de Lesegno and Hennequin can be considered unlikely at low collision energies.

Taking into account also the different Ar Auger transition rates in the Ar-Si and Ar-Mg (Ar-Al) cases,[17] we propose that both symmetric collisions between the projectile Ar particles and preimplanted Ar atoms in the Si matrix and asymmetric encounters between Ar and Si atoms are responsible for the production of the Ar $2p$ holes. In particular, for this latter case we suggest that a Si target atom doubly excited in a violent collision with an impinging Ar can decay through a two-electron process in a subsequent encounter with an implanted Ar atom in which one of the Si two $2p$ vacancies is filled by a valence electron and the energy is used to simultaneously transfer an Ar $2p$ electron to the other empty Si L shell. The energy of a Si $2p^43s^23p^2$ state can be roughly estimated to be 259 eV using the $Z+1$ rule, very close to the free Ar $2p$ binding energy of 248.6–250.6 eV (Ref. 25). Considering the large uncertainty in the first value and a possible degeneracy of the energy levels during the collision, such a process is energetically allowed.

Inter-atomic transitions in heavy particle collisions have been observed by Legg, Metz, and Thomas[19] for Ar transition-metal systems and recently been observed by Valeri and Verucchi[36] for Ar^+-Cr even at primary energy as low as ~ 15 keV. Calculations on the cross section for such transitions are beyond the purpose of this paper, and we only consider this mechanism energetically possible. The proposed Si^{2*}-Ar collision mechanism also provides an interpretation to the very different intensity behavior in the Ar-Si and Ar-Mg (Ar-Al) cases where the concentration of implanted Ar is very similar.[17] In fact,

such processes cannot be effective in these latter cases because of the large discrepancies in the binding energies of the Ar $2p$ level and in the Mg or Al double L-shell vacancies (Mg $2p^4 3s^2$: ~ 146 eV and Al $2p^4 3s^2 3p^1$: ~ 199 eV).[37] If this mechanism is indeed active in Si^{2*}-Ar collisions, then the ratio between the excitation events in symmetric and asymmetric encounters should be collision energy dependent. Previous studies have established that a double inner-shell vacancy in Si can be produced merely by asymmetric encounters with Ar^+ ions or Ar atoms.[38,39] Considerations based on the small Ar implantation concentration in Si and the reduced collision energies in implanted Ar-Si encounters lead us to argue that the only possible Si^{2*} excitation–Si^{2*} to Ar L-shell vacancy transfer process for the creation of $2p$ vacancy in Ar is the projectile Ar^+ (Ar)-Si–Si^{2*}-implanted Ar collision sequence. The excitation of the Ar $2p$ electron in both symmetric and asymmetric collisions is limited by the concentration of implanted Ar. However, the increase in the probability of the double Si inner-shell excitation is much more pronounced than that in the core excitation in Ar (the results of Fig. 7 indicate that the Si L_{23}^2-$L_{23}M_{23}^2$ signal increases not only faster than those of the single Ar $L_{23}M_1M_{23}$ and $L_{23}M_{23}M_{23}$ components but also faster than the total Ar Auger intensity).

C. The case of Ar^+-Ti

In this case, it is expected that in an asymmetric collision between Ar and Ti, the $2p$ electron in Ar is excited through $4f\sigma$ molecular-orbital radial couplings so that a larger LMM signal can be detected. The smaller work function relative to Si would also suggest stronger surface neutralization effects for the incoming Ar^+ ions.

In Fig. 1 we show a representative Ar spectrum taken in the $N(E)$ mode. In Fig. 8 we present a set of normalized derivative Ar Auger spectra for various primary ion energies E_p and for $\theta_i = 45°$ (left panel) and four spectra taken at different incidence and detection angles (in our experimental layout $\theta_i + \theta_e = 70°$) for a fixed $E_p = 15$ keV (right panel).

We notice that the main $L_{23}M_{23}M_{23}$ peak in the electron-induced Auger spectrum (EIAS) is situated at 211.9 ± 0.3 eV, very similar to that for Ar embedded in Si. However, the relative intensity of the $L_{23}M_1M_{23}$ feature is greatly reduced with respect to the cases of Ar^+-Ar and Ar^+-Si (see the upper panel of Fig. 5), again indicating a strong matrix effect on the relative transition rates. The structure seen at 227 ± 1 eV can be attributed to an $L_{23}M_{23}V$ interatomic transition involving one valence electron of the Ti matrix or an autoionization $L_{23}M_{23}N_1$ in a neutral Ar atom while that at 239 ± 1 can be assigned to an $L_{23}VV$ transition.

The negative cursor of the most intense peak $L_{23}M_{23}M_{23}$ in ion-induced Auger spectra (IIAS) is shifted for 2–3 eV toward higher kinetic energy whereas the positive cursor remains essentially unaltered. An inflation at about 211 eV indicates that this peak is actually composed of two components, one due both to decay occurring in the bulk and in vacuum from slow-moving Ar species and one at higher energy due to deexcitation

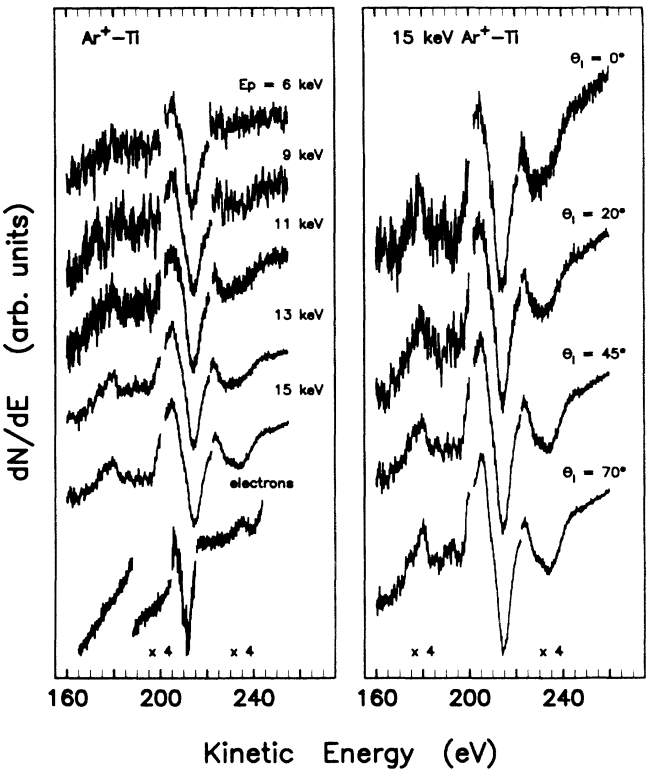

FIG. 8. Normalized Ar Auger spectra obtained by impinging Ar^+ ions on a Ti sample for various primary ion energies E_p and for $\theta_i = 45°$ (left panel) and for 15-keV Ar^+ ion impact at four incidence angles (right panel). In our experimental layout the analyzer is fixed at 70° with respect to the beam direction. Features with weaker intensities at lower- and higher-energy sides have been appropriately magnified. The bottom-most curve is that for electron impact on Ar implanted in Ti.

of fast-moving particles outside the sample. The atomic-like character of the latter is clearly confirmed by the Doppler shift of its peak position from 213.5 eV at $E_p = 6$ keV to 214.9 eV at 15 keV (left panel of Fig. 8). The absence of a downward shift of the positive cursor clearly indicates that, unlike in the Ar^+-Ar and Ar^+-Si cases, virtually all the impinging Ar^+ projectile ions are neutralized by surface conduction electrons before or after collisions with the target Ti atoms.

The relative intensities of the two peaks at 228 ± 1 and 233 ± 1 eV vary gradually with the primary energy and the incidence angle. We propose that the most probable candidates for the first peak at 228 eV can be an $L_{23}M_{23}V$ transition, just as in the case of electron impact, or an $L_{23}M_{23}N_1$ one decaying in the solid.

For the second peak at 233 ± 1 eV, we suggest that it can result from the L_{23}^2-$L_{23}M_1N_1$ decay from an initially doubled excited L_{23}^2 state. The energy of the L_{23}^2 state can be obtained from the calculations of Larkins[32] while that for the autoionizing configuration $2p^{-2}$-$4s^1$ can be easily estimated with the $Z+1$ model.[40] The theoretical prediction of the kinetic energy of this transition is 232 eV. Taking into account its large uncertainty we may consider it in good agreement with the experimental value which is affected also by the Doppler effect. It has

been demonstrated previously for Mg, Al, and Si that for low-energy (close to the threshold) collisions the Auger intensity ratio between the doubly and singly excited features increases monotonously with the primary energy.[38,39] The energy-dependent behavior of the relative intensity (Fig. 8) of this peak fully respects this general trend.

The 4s binding energy in an inner-shell doubly excited Ar ion is about 10.9 eV, considerably larger than the Ti surface work function. Therefore, a substantial portion of the outgoing doubly excited Ar^{2*} ions can capture a solid free electron into its 4s outer shell. An increase in the collision energy will enhance the probability of excitation of an inner double vacancy but will reduce that for charge transfer from the solid to the empty 4s level (this mechanism is expected to prevail on direct 2p-4s transitions) for a fixed experimental geometry. The observed primary energy dependence of the relative intensity of the L_{23}^2-$L_{23}M_1N_1$ peak is just a result of these two competing effects.

The lowest-energy structure at ~169 eV shows a strong dependence on the incidence angle. For normal incidence, this peak is quite intense and well resolved from the background. As discussed in Sec. III A, it can be due to an overlap of many unresolved transition lines from an initial $2p^{-1}3s^{-1}$ state to a final $3s^{-2}3p^{-1}$ configuration.[13,28]

Auger decays involving one or two 3s electrons have nearly the same intensities. The angular dependence of the $L_{23}M_1M_{23}$ to $L_{23}M_{23}M_{23}$ intensity ratio indicates a possible variation of the portion of the decay processes occurring inside and outside the solid. The spectra shown in Fig. 8 suggest that the relative probability of the participation of one or two M_1 electrons in the decay of the L_{23} vacancy increases with collision energy, a behavior somehow similar to, though much less pronounced than, that observed for Ar^+-Si. For a better comparison, we illustrate in the lower panel of Fig. 5 the Ar Auger spectra obtained for three different collision systems. This phenomenon and the surface neutralization effects constitute two unique aspects of the Auger-electron emission in ion-solid interactions and provide a possible interpretation for the observed very different relative transition ratios.

In Fig. 7 we plot the total Ar L-shell Auger intensities as a function of the primary ion energy. These results show the very different energy dependence relative to the Ar^+-Si system. In an angle-resolved line-shape analysis for an analogous Ne^+-Ar system, Pepper[41] demonstrated that practically all the excitation events leading to Auger decay in the vacuum occur in the primary projectile-target encounters. We believe that this could be the case also for the Ar-Ti system.

IV. CONCLUSIONS

In summary, we have studied Ar L-shell Auger-electron emission produced by Ar^+ ion bombardment on solid Ti, Si, and condensed Ar layer surfaces. The most salient conclusions can be summarized in the following.

(1) The great majority of Auger decays of the Ar L-shell vacancies involves its own outer shell electrons instead of matrix valence electrons. The kinetic energies of the emitted LMM Auger electrons and the relative transition ratios are sensitively influenced by the chemical nature of the surrounding environment.

(2) Most of the projectile Ar^+ ions impinging on a metallic surface are neutralized before or after hitting the target surface through either a resonant tunneling or an Auger neutralization process by capturing a free electron of the solid. For Ar-Si and Ar-condensed Ar/Al, a non-negligible portion of the inner-shell-excited leaving Ar particles can still have a 3p vacancy in such a way that the Auger decays are characterized as the $L_{23}M_{23}$-M^3 satellite lines. The relative weight of these features with respect to the normal $L_{23}MM$ transitions depends on the surface nature and on the surface conditions.

(3) The intensity ratio between transitions involving one and no 3s electrons differs from the value observed for electron impact. Such intensity ratio varies with the collision energy if the deexcitation occurs in the solid. These results demonstrate the peculiarities of the deexcitation process in ion-solid interactions with respect to the gas-phase experiments.

(4) We have proposed that excitation of the 2p electron of Ar in the case of Ar-Si can be produced in both symmetric projectile Ar-implanted Ar collisions and asymmetric Ar-Si collisions. In particular, we suggested a two-electron process for the latter ones in which one of the two 2p holes of a Si atom excited in a previous Ar-Si encounter is filled by an outer shell or valence electron and the released energy is used for electron transfer from the L shell of an Ar atom to the other hole in Si.

(5) Various high-energy peaks are observed in three different systems. The kinetic energies of these features differ from each other and our detailed analysis reveals that they belong to different transitions, characteristic of each particular system.

ACKNOWLEDGMENTS

We thank E. Li Preti and V. Fabio for technical collaboration. This work was partially supported by CNR under contract of Progetto Finalizzato-Materiali Speciali per Tecnologie Avanzate and by Istituto Nazionale de Fisica Nucleare (INFN), Unità di Losenza.

[1]N. Stolterfoht, Phys. Rep. **146**, 315 (1987).
[2]U. Wille and R. Hippler, Phys. Rep. **132**, 129 (1986).
[3]J. A. D. Matthew, Phys. Scr. **T6**, 79 (1983).
[4]E. W. Thomas, Vacuum **34**, 1031 (1984).
[5]U. Fano and W. Lichten, Phys. Rev. Lett. **14**, 627 (1965).
[6]M. Barat and W. Lichten, Phys. Rev. A **6**, 211 (1972).
[7]H. D. Hagstrum, Phys. Rev. **96**, 336 (1954).
[8]H. D. Hagstrum, in *Inelastic Ion-Surface Collisions*, edited by N. H. Tolk, J. C. Tully, W. Heiland, and C. W. White (Academic, New York, 1977).

[9]G. Zampieri, F. Meier, and R. Baragiola, Phys. Rev. A **29**, 116 (1984).
[10]O. Grizzi, M. Shi, H. Bu, J. W. Rabalais, and R. A. Baragiola, Phys. Rev. B **41**, 4789 (1990).
[11]G. N. Ogurtsov, I. P. Flaks, and S. V. Avakyan, Zh. Eksp. Teor. Fiz. **57**, 27 (1969) [Sov. Phys. JETP **30**, 16 (1970)].
[12]D. J. Volz and E. M. Rudd, Phys. Rev. A **2**, 1395 (1970).
[13]N. Stolterfoht, D. Schneider, and P. Ziew, Phys. Rev. A **10**, 81 (1974).
[14]B. M. Johnson, D. L. Matthews, L. E. Smith, and C. F. Moore, J. Phys. B **16**, L369 (1973).
[15]D. Schneider, B. M. Johnson, B. Hodge, and C. F. Moore, Phys. Lett. **59A**, 25 (1976).
[16]J. Kempf and G. Kaus, Appl. Phys. **13**, 261 (1977).
[17]P. Viaris de Lesegno and J. F. Hennequin, Surf. Sci. **80**, 656 (1979).
[18]P. Viaris de Lesegno and J. F. Hennequin, J. Phys. (Paris) **35**, 759 (1974).
[19]K. O. Legg, W. A. Metz, and E. W. Thomas, Nucl. Instrum. Methods **170**, 561 (1980); J. Appl. Phys. **51**, 4437 (1980).
[20]K. Wittmaack, Phys. Lett. **74A**, 197 (1979).
[21]M. E. Rudd, T. Jorgensen, Jr., and D. J. Volz, Phys. Rev. **151**, 28 (1966).
[22]N. Stolterfoht, D. Schneider, and H. Gabler, Phys. Lett. **47A**, 271 (1974).
[23]L. O. Werme, T. Bergmark, and K. Siegbahn, Phys. Scr. **8**, 149 (1973).
[24]*Handbook of Physics and Chemistry,* 65th ed. (CRC, New York, 1985).
[25]M. Nakamura *et al.*, Phys. Rev. Lett. **21**, 1303 (1968).
[26]A. R. Striganov and N. S. Sventitskii, *Tables of Spectral Lines of Neutral and Ionized Atoms* (IFI/Plenum, New York, 1968).
[27]E. Bertel, R. Stockbauer, and T. E. Madey, Phys. Rev. B **27**, 1939 (1983).
[28]A theoretical prediction of 163.3 eV, relative to the vacuum level, for the $2p^{-1}3s^{-1}$-$3s^{-2}3p^{-1}$ transition can be obtained by using the energy calculations of Larkins (Ref. 32).
[29]Gas-phase e^--Ar experiments (Ref. 23) give a set of transitions in the energy range between 191.6 and 196.7 eV (in the integral mode). More significantly, the energy difference of 10.5–16.6 eV between this peak and the main $L_{23}M_{23}M_{23}$ one fits quite well our data if we take into account that the peak position is greatly influenced by the overlap with the $L_{23}M_{23}M_{23}$ peak and a probably larger Doppler shift. The largest separation observed at $E_p=9$ keV amounts to ~ 10 eV.
[30]G. M. Thomson, P. C. Laudieri, and E. Everhart, Phys. Rev. A **1**, 1430 (1970).
[31]G. F. Zampieri and R. A. Baragiola, Surf. Sci. **114**, L15 (1982).
[32]F. P. Larkins, J. Phys. B **4**, 1 (1971).
[33]R. A. Baragiola, L. Nair, and T. E. Madey, Nucl. Instrum. Methods **B58**, 322 (1991).
[34]G. M. Thomson, Phys. Rev. A **15**, 865 (1977).
[35]D. Schneider, G. Nolte, U. Wille, and N. Stolterfoht, Phys. Rev. A **28**, 161 (1983).
[36]S. Valeri and R. Verucchi, Phys. Scr. **T41**, 246 (1992).
[37]For a discussion on the $Z+1$ model see P. Dahl, M. Rodbro, G. Hermann, B. Fastrup, and M. E. Rudd, J. Phys. B **9**, 1581 (1976) and R. Whaley and E. W. Thomas, J. Appl. Phys. **56**, 1505 (1984).
[38]F. Xu, M. Camarca, A. Oliva, N. Mandarino, P. Zoccali, and A. Bonanno, Surf. Sci. **247**, 13 (1991).
[39]F. Xu, F. Ascione, N. Mandarino, P. Zoccali, P. Calaminici, A. Oliva, A. Bonanno, and N. Russo (unpublished).
[40]If we apply this rule, we have $E(\text{Ar } 2p^4 3s^2 3p^6 4s^1) - E(\text{Ar } 2p^4 3s^2 2p^6) = E(K\,2p^5 3s^2 3p^6 4s^1) - E(\text{K } 2p^5 2s^2 3p^6) = E(\text{Ca } 2p^6 3s^2 3p^6 4s^1) - E(\text{Ca } 2p^6 3s^2 3p^6)$; thus $E(\text{Ar } 2p^4 3s^2 3p^6 4s^1) = 529.1$ eV.
[41]S. V. Pepper, Surf. Sci. **169**, 39 (1986).